

# Diffusion of Single Streptocyanine Molecules in the Nanoporous Network of Sol–Gel Glasses<sup>†</sup>

Christian Hellriegel,<sup>‡</sup> Johanna Kirstein,<sup>‡</sup> Christoph Bräuchle,<sup>\*,‡</sup> Virginie Latour,<sup>§</sup> Thierry Pigot,<sup>§</sup> Rémi Olivier,<sup>§</sup> Sylvie Lacombe,<sup>§</sup> Ross Brown,<sup>\*,§</sup> Valérie Guieu,<sup>⊥</sup> Corinne Payraastre,<sup>⊥</sup> Albert Izquierdo,<sup>⊥</sup> and Pierre Mocho<sup>#</sup>

Department Chemie and CeNS, Ludwig-Maximilians Universität München, Butenandtstr. 11, 81377 München, Germany, Laboratoire de Chimie Théorique et de Physico-Chimie Moléculaire, umr 5624 du CNRS et de l'Université de Pau et des pays de l'Adour, IFR, rue Jules Ferry, 64075 Pau Cedex, France, Laboratoire de Synthèse et de Physico-Chimie de Molécules d'Intérêt Biologique, umr 5068 du CNRS et de l'Université Paul Sabatier de Toulouse, 118 route de Narbonne, 31062 Toulouse Cedex 04, France, and Laboratoire de Thermique Énergie et Procédés, Université de Pau et des pays de l'Adour, Avenue de l'Université, B.P. 1155, 64013 Pau Cedex, France

Received: February 9, 2004; In Final Form: April 29, 2004

A new streptocyanine dye has been doped into monolithic silica gels with different porosities, characterized by nitrogen adsorption isotherms. Single-molecule tracking with a wide-field fluorescence microscope is used to determine the diffusivity of the dye in the nanoporous network of the host. The majority of molecules in the gel with wider pores (22 nm) diffuse freely with an average diffusion coefficient of  $D = 4.7 \times 10^{-9} \text{ cm}^2 \text{ s}^{-1}$ . Most of those in the gel with narrower pores (3 nm) are trapped in regions ranging in size from 50 nm—the positioning accuracy of the setup—up to 200 nm. Others are alternately trapped and freely diffusing with an average  $D = 3.5 \times 10^{-10} \text{ cm}^2 \text{ s}^{-1}$ . The significance of the distribution of diffusion coefficients measured by single-molecule tracking is discussed. Besides traps, the wide spread of the diffusion coefficients for individual molecules in both gels reveals pronounced microscopic inhomogeneities.

## 1. Introduction

Hybrid materials in which an organic guest molecule is encapsulated in a mineral host have many and varied applications, including biological and environmental sensors,<sup>1</sup> laser media<sup>2–4</sup> and nonlinear optical devices,<sup>5</sup> and photocatalysis.<sup>6</sup> In many metal-catalyzed industrial reactions, diffusion of reactants into the porous silica used to support the metal clusters is also of importance.<sup>7</sup> Hybrid materials are prepared either by encapsulating the active compound during synthesis, or in the case of suitably porous materials, by adsorbing it from solution after synthesis. Among these materials, amorphous, micro- and mesoporous silicas are widely used as hosts because they are cheap and easy to prepare by sol–gel synthesis in a variety of physical forms, including powders, cast monoliths, and spin-coated thin films. Porous sol–gel materials may also perform size-selective separations, molecular recognition, or contribute to stabilization of reactive species. It is therefore of some interest to gain a microscopic view of interactions between the guest and the host.

Molecular diffusion in micro- and mesoporous materials has been the subject of many experimental investigations, using techniques such as pulsed field gradient NMR,<sup>8</sup> quasi-elastic neutron scattering,<sup>9,10</sup> vibrational spectroscopy,<sup>11,12</sup> fluorescence

anisotropy,<sup>13,14</sup> excimer fluorescence,<sup>15,16</sup> or fluorescence recovery after bleaching.<sup>17</sup> The problem is that although the distribution of pore sizes in silica gels may be controlled to some extent by varying the conditions of synthesis, notably the pH and amount of excess water, we know from, for example, transmission electron micrographs, that there is a distribution of pore sizes and shapes.<sup>18</sup> Pore sizes are often inferred from analysis of adsorption isotherms for nitrogen or other gases, which requires assumptions about pore shapes and may not be pertinent to adsorption of large organic molecules used in applications. For example, bottlenecks between pores might close off regions of the pore system accessible to adsorption of smaller molecules such as nitrogen. Furthermore, one expects that Brownian motion of large organic molecules in a gel will be sensitive to local properties such as the surface curvature and roughness on an atomic scale, pore connectivity, or local fluctuations in the surface chemistry of amorphous silica, leading to a range of adsorption energies, influencing Brownian motion.

The ensemble techniques mentioned above provide only an average diffusion coefficient or at best an indication of a spread of values through nonexponential relaxation of parameters such as the fluorescence anisotropy. There is therefore a need for methods that can resolve the local fluctuations. Fortunately, the high sensitivity of fluorescence measurements can be put to use to study interactions of very small numbers of molecules with the substrate, down to single-molecule sensitivity. In such measurements, laser-induced emission of the guest molecules embedded in the transparent host is recorded in some form of optical microscopy. Molecular diffusion can be evaluated in two ways. The first is statistical analysis of the fluctuations of the fluorescence signal when molecules diffuse in and out of a fixed

<sup>†</sup> Part of the special issue "Gerhard Ertl Festschrift".

<sup>\*</sup> Corresponding authors. E-mail: Christoph.Braeuchle@cup.uni-muenchen.de (C.B.); ross.brown@univ-pau.fr (R.B.).

<sup>‡</sup> Ludwig-Maximilians Universität.

<sup>§</sup> Laboratoire de Chimie Théorique et de Physico-Chimie Moléculaire, Université de Pau et des pays de l'Adour.

<sup>⊥</sup> Université Paul Sabatier de Toulouse.

<sup>#</sup> Laboratoire de Thermique Énergie et Procédés, Université de Pau et des pays de l'Adour.

focal volume, as in fluorescence correlation spectroscopy,<sup>19,20</sup> a technique now widely applied to measurement of molecular diffusion in plant or animal cells and membranes.<sup>21</sup> This technique allows measurement of diffusion coefficients over a wide range, from about  $10^{-8}$  cm<sup>2</sup> s<sup>-1</sup> to  $10^{-4}$  cm<sup>2</sup> s<sup>-1</sup>. A disadvantage, for the analysis of such complicated systems as organic molecules in silica gels, is that the fluorescence correlation function,  $g^{(2)}(\tau) = \langle I(t) I(t + \tau) \rangle \langle I(t) \rangle^{-2}$ , where  $I(t)$  is the instantaneous intensity, has to be matched to an a priori expression derived from a model of the diffusion process, including aspects such as free or hindered diffusion or the presence of several kinds of adsorption sites with different strengths.

The second, conceptually more straightforward, but slower method, is to record sequences of images of very dilute samples. Single molecules appear as diffraction-limited bright spots which may move from frame to frame.<sup>22–24</sup> The motion of each molecule is recovered from analysis of the spots in successive images. This approach allows detailed study of diffusion.<sup>22,25</sup> Naturally, the time range that can be covered is restricted by the need to expose each frame long enough to obtain unambiguous single-molecule images. There are two main reasons why single-molecule detection is nonetheless particularly appealing for probing diffusion in materials such as doped sol–gels. The first is that single-molecule detection yields a complete distribution of a parameter such as the diffusion coefficient, rather than just the average value.<sup>26–28</sup> For example, the distribution of the tilt angle of individual molecules of an oxazine dye in a microporous molecular sieve has been determined by single-molecule detection.<sup>29</sup> As will be shown below, single-molecule detection can also distinguish non-Brownian behavior of individual molecules, when the ensemble behavior appears normal. The second advantage is that a single molecule is the ultimate probe of spatial inhomogeneities.

Several papers have reported applications of these techniques to silica-based materials. Wirth and co-workers<sup>30,31</sup> measured the fluorescence correlation of a carbocyanine dye adsorbed on chromatographic interfaces, consisting of amorphous silica derivatized with an alkyl silane monolayer. They distinguished diffusing molecules and several types of adsorption, from photon bursts lasting from 70 ms to several seconds. Mei et al.<sup>32</sup> studied rhodamine B in spin-coated silica gel films. They reported fluorescence correlation measurements, images of immobile single molecules and their spectra, in spin-coated films at different stages of drying. Fluorescence correlation spectroscopy was applied by Mahurin et al.<sup>33</sup> to rhodamine 6G adsorbed in a porous glass. Their data indicated a spread of diffusion coefficients, or a mixture of mobile and trapped particles. Seebacher et al.<sup>34</sup> examined a templated mesoporous silica gel (M41S), doped with a terylene diimide derivative. The guest diffused in tubular micelles of the template, encased in millimeter-sized monolithic silica. Diffusion coefficients derived from tracking of single molecules were 2 orders of magnitude lower than those found by fluorescence correlation spectroscopy in the micellar mesophase before introducing silica. Single-molecule detection does have drawbacks for measuring diffusion. One is that tracks are often very short, only a few steps, owing either to photobleaching or to diffusion out of the focal volume of the microscope. Short tracks lead to poor statistics, unless their shortness can be compensated by tracking more molecules. Fast moving molecules or ones with a low fluorescence yield may be difficult to follow because of low signal-to-noise ratios and inaccurate positions. In a study of a dip-coated silica gel film, McCain et al.<sup>35</sup> nonetheless succeeded in

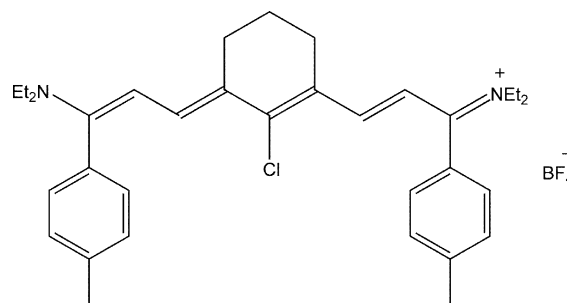


**Figure 1.** Chemical structure of streptocyanine 9A1, 5-chloro-1,9-diethylamino-1,9-di(4-methylphenyl)-4,6-[propane]-nona-1,3,5,7-tetraenylum tetrafluoroborate.

recording diffusion of single molecules of rhodamine 6G, with a temporal resolution of 0.8 s and a positioning accuracy below 130 nm. These authors found significantly different diffusion coefficients for five molecules in different parts of the sample.

In this paper we focus on the influence of pore size on molecular diffusion in cast silica xerogels and on spatial heterogeneities in these systems. Two types of xerogel were doped with a new streptocyanine dye, encapsulated during synthesis of the monoliths. In one of the gels the pores are about the same size as the dye molecule; in the other they are much bigger. Diffusion of single molecules is studied by particle tracking under a far field microscope with high spatial (50 nm) and temporal (50 to 100 ms) resolution. Statistics are established from about 50 molecules in each type of gel. Section 2 describes the materials and methods. The results are presented, analyzed statistically, and discussed in section 3. Section 4 contains the main conclusions.

## 2. Experimental Section

**2.1. Synthesis of the Streptocyanine 9A1.** Polymethinium dyes are cationic conjugated organic compounds containing an odd-numbered chain of carbon atoms between two nitrogens. In cyanines, the nitrogen atoms are in conjugated heterocycles. In streptocyanines they are not. These dyes have a number of uses, such as photosensitizers, laser dyes, and biological fluorescent labels. The wavelengths of the absorption and emission maxima can be finely tuned across the visible and infrared spectrum by changing the length of the conjugated chain and the terminal substituents. Compound 9A1 (5-chloro-1,9-diethylamino-1,9-di(4-methylphenyl)-4,6-[propane]-nona-1,3,5,7-tetraenylum tetrafluoroborate, see Figure 1), was synthesized by action of 2 equiv of diethylamine on a carboxonium salt, 5-chloro-1,9-diethoxy-1,9-di(4-methylphenyl)-4,6-[propane]nona-1,3,5,7-tetraenylum tetrafluoroborate.<sup>36,37</sup> Synthesis was done under dry conditions (argon atmosphere, anhydrous solvents) to avoid degradation of the carboxonium salt. In the first step, 0.21 mL (2.08 mmol) of diethylamine was added drop by drop to 5-chloro-1,9-diethoxy-1,9-di(4-methylphenyl)-4,6-[propane]nona-1,3,5,7-tetraenylum tetrafluoroborate (0.571 g, 1.04 mmol) in 100 mL of anhydrous acetonitrile. The solution was stirred for 24 h at room temperature and then filtered off to eliminate the unreacted diketone. The solvent was then removed under reduced pressure, and the crude streptocyanine was recrystallized from ethanol.

The melting point was determined with a Büchi capillary apparatus. <sup>1</sup>H NMR and <sup>13</sup>C NMR spectra were recorded on a Bruker AC 250 or a AM 400 WB spectrometer. Chemical shifts are given in ppm from tetramethylsilane. The mass spectrum was recorded on a Nermag R10-10H spectrometer. The absorption spectrum was recorded on a Hewlett-Packard 8453 UV–

vis spectrometer. Excitation and fluorescence emission spectra were measured on a Perkin-Elmer LS 50B spectrofluorimeter. Elemental analysis was done at the Interuniversity Microanalysis Service of the Chemistry School of Toulouse (ENSIACET).

The properties of 9A1 are as follows: green, rod shaped crystals, length 250  $\mu\text{m}$ , diameter 30  $\mu\text{m}$ , (82%), mp: 235–237  $^{\circ}\text{C}$  (dec).  $^1\text{H}$  NMR (400 MHz,  $\text{CDCl}_3$ , 25  $^{\circ}\text{C}$ )  $\delta$  = 1.19 (m, 12H,  $(\text{CH}_3-\text{CH}_2)_2-\text{N}$ ); 1.78 (quint, 2H,  $^3J$  = 6.0,  $\text{H}_{5'}$ ); 2.35 (s, 6H,  $\text{CH}_3-\text{Ar}$ ); 2.46 (t, 4H,  $^3J$  = 6.0,  $\text{H}_{4'-6'}$ ); 3.46 (m, 8H,  $^3J$  = 13.2,  $(\text{CH}_3-\text{CH}_2)_2-\text{N}$ ); 5.98 (d, 2H,  $^3J$  = 13.2,  $\text{H}_{2-8}$ ); 7.03 (part A from an AB syst, 4H,  $^3J$  = 8.2,  $\text{H}_{\text{arom}}$ ); 7.05 (d, 2H,  $^3J$  = 13.2,  $\text{H}_{3-7}$ ); 7.21 (part B from an AB syst, 4H,  $^3J$  = 8.2,  $\text{H}_{\text{arom}}$ ) ppm.  $^{13}\text{C}$  NMR Jmod  $^{13}\text{C}\{^1\text{H}\}$  (100 MHz,  $\text{CDCl}_3$ , 25  $^{\circ}\text{C}$ )  $\delta$  = 21.1 ( $\text{CH}_2(5')$ ); 21.6 ( $\text{CH}_3-\text{Ar}$ ); 27.0 ( $\text{CH}_2(4'-6')$ ); 106.0 ( $\text{CH}_2-8$ ); 124.4 ( $\text{C}_{4-6}$ ); 128.5 ( $\text{CH}_{\text{arom}}$ ); 129.6 ( $\text{CH}_{\text{arom}}$ ); 130.6 ( $\text{C}_{\text{arom}}-\text{C}_{1-9}$ ); 140.3 ( $\text{C}_{\text{arom}}-\text{CH}_3$ ); 150.0 ( $\text{CH}_{3-7}$ ); 150.7 ( $\text{C}_5-\text{Cl}$ ); 167.8 ( $\text{C}_{1-9}$ ) ppm. MS (electrospray):  $m/z$  (%) = 515.2 (100)  $[\text{M}]^+$ ,  $\text{C}_{34}\text{H}_{44}\text{BClF}_4\text{N}_2$  (602.99). Calcd C 67.72, H 7.35, N 4.65; found C 67.84, H 7.15, N 4.56. Absorption (23  $^{\circ}\text{C}$ ,  $\text{CH}_2\text{Cl}_2$ ):  $\lambda_{\text{max}}$  nm ( $\epsilon_{\text{max}}$   $\text{M}^{-1} \text{cm}^{-1}$ ) shoulder at 643, 695 (240 000). Fluorescence spectrometry (23  $^{\circ}\text{C}$ ,  $\text{CH}_2\text{Cl}_2$ ):  $\lambda_{\text{ex}}/\lambda_{\text{em}}$ , 686/719 nm.

**2.2. Sample Synthesis and Mounting.** Silica monoliths were obtained by the conventional method of hydrolysis and condensation of tetramethyl orthosilicate (TMOS) in the presence of methanol, under neutral conditions.<sup>18</sup> After some experimentation it was found that samples suitably clear and crack-free for single-molecule detection could be obtained with the procedure below. Samples of different porosity were obtained, depending on the TMOS/methanol/water molar ratio, which was here 1/5/4 or 1/5/20. The resulting gels are called here M22 and M3, after their pore sizes in nm, determined below. The initial ratio of water to TMOS (water is also produced during condensation of the silicate) is stoichiometric for M22 but corresponds to a large excess of water for M3. The purity of all materials was checked by fluorescence spectroscopy on a Perkin-Elmer LS 50B spectrofluorimeter. A dilution series of the dye 9A1 was prepared in methanol (SDS, spectrophotometric grade), at concentrations adjusted so that, allowing for shrinkage of the gels during drying (about 80%), the final concentrations in the monoliths were in the range of  $5 \times 10^{-7}$  to  $5 \times 10^{-13}$  M. The solutions in methanol were added to unbuffered water (reverse osmosis, 5 to 10  $\mu\text{S cm}^{-1}$ ), and TMOS (Aldrich, 99%) was added in one step. This solution was stirred magnetically for 2 min. Samples of 1 mL of the sol were closed in polypropylene Eppendorf microtubes. Gelation was achieved in 10 days in an oven at 50  $^{\circ}\text{C}$ . The microtubes were then opened for drying the gels at atmospheric pressure for 6 h at 60  $^{\circ}\text{C}$  and 60 h at 80  $^{\circ}\text{C}$ , after which the samples were kept in the closed tubes until use. Residual water and methanol are present in the dried monoliths. The loss of solvent on further drying under primary vacuum for 4 h at 200  $^{\circ}\text{C}$  was about 15% of the dry weight, or a volume corresponding to the common micropore volume of the gels (see below).

Nitrogen adsorption and desorption isotherms of the gels were measured at 77 K on a Micromeritics ASAP 2010 Micropore nitrogen adsorption apparatus. The isotherms of gel M3 are of type I (Langmuir model, monolayer adsorption) in the BDDT classification<sup>38</sup> (see Figure 2). M22 gels have type IV (BET model, multilayer) isotherms. The hysteresis between desorption and adsorption in M22 is characteristic of a mesoporous material. Both materials have micro- (diameter under 2 nm) and mesopores (diameter 2–50 nm). The isotherms of M3 and M22 are very close in the range  $p/p_0 < 0.3$ , indicating a similarity

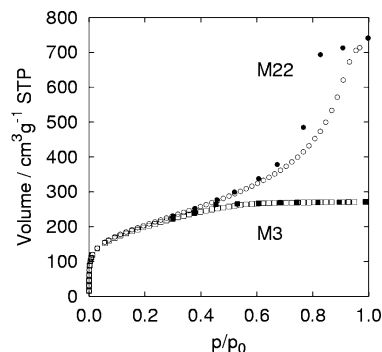


**Figure 2.** Analysis of the porosities of the xerogels. Nitrogen adsorption (open symbols) and desorption (filled symbols) isotherms at 77 K, for the silica xerogels M3 (squares) and M22 (circles). The gels have very similar microporosities, but M22 has a significantly larger mesoporosity (see Table 1).

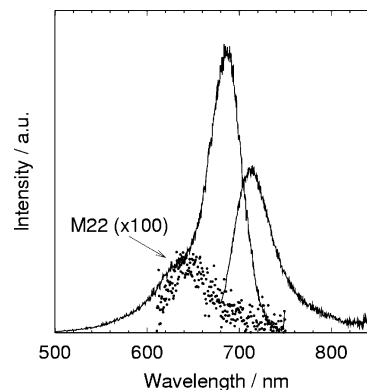


**Figure 3.** Fluorescence and excitation spectra of 9A1 at a concentration of ca.  $10^{-7}$  M in methanol, and the emission spectrum in the M22 xerogel at the same concentration.

**TABLE 1: Porosity Data for Silica Gels M3 and M22**

gel	M3	M22
Brunauer–Emmett–Teller <sup>44</sup> specific surface area ( $\text{m}^2 \text{g}^{-1}$ )	715	740
Horvath–Kawazoe <sup>45</sup> slit micropore volume ( $\text{cm}^3 \text{g}^{-1}$ )	0.25	0.25
Barrett–Joyner–Halenda <sup>46</sup> mesopore volume ( $\text{cm}^3 \text{g}^{-1}$ )	0.15	0.9
BJH mesopore surface area ( $\text{m}^2 \text{g}^{-1}$ )	200	160
H–K median micropore diameter (nm)	0.8	0.8
BJH mean mesopore diameter (nm)	3.1	22.4

of microporosities ( $p/p_0 < 0.01$ ) extending well into the mesopore range. The micropore volume is in fact the same for M3 and M22 (Table 1). Mesoporosity in gel M3 is limited ( $0.15 \text{ cm}^3 \text{g}^{-1}$ ) but is much larger ( $0.9 \text{ cm}^3 \text{g}^{-1}$ ) in M22. Table 1 summarizes the principal data deduced from the isotherms. Gel M22, with a wide spread of mesopore diameters (mean 22.4 nm), was less well described than M3 by the BJH model, and the figures given for its mesoporosity should be taken as approximate.

The fluorescence and excitation spectra of 9A1 in methanol, water, and ethylene glycol (see below) and in the monoliths were recorded with an Edinburgh FS920 spectrofluorimeter. The spectra in water and ethylene glycol are very close to those in methanol, shown in Figure 3. The fluorescence spectrum in the monoliths was substantially blue shifted compared to those in methanol solution (see Figure 3). It was also about 2 orders of magnitude weaker in the monoliths than in solution. This effect was not found for monoliths doped with other dyes examined in the same gels in the same experimental geometry and conditions and must therefore reflect a reduced average fluorescence. Since single molecules could be observed with high counting rates in the single-molecule setup, it is possible that



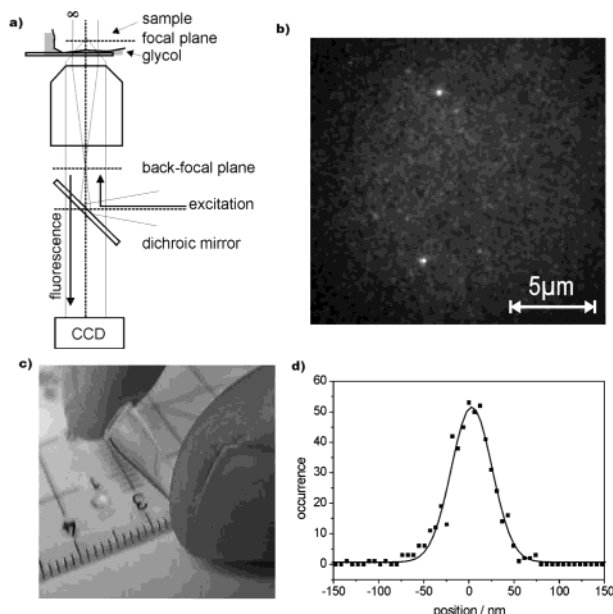


**Figure 4.** Experimental setup and image recording. (a) Schematic drawing of the wide-field imaging setup; (b) a typical image recorded with the setup, showing diffraction-limited fluorescence spots of two individual molecules of 9A1 in M3; (c) picture of a monolithic cast silica xerogel; (d) distribution of the fluctuations of the coordinate of an immobile molecule due to noise, in a film of 500 frames. The standard deviation of 22.1 nm confirms the accuracy of the positioning error, which is 21.2 nm for this molecule.

the fluorescence quantum yield of a majority of molecules is very low compared to the value in solution. One explanation for the weak fluorescence and the blue shift in the gel compared to the solution is a reduction of conjugation due to deformation of the molecule in the solid. It is possible that a majority of molecules are adsorbed in narrow pores, for which one would expect both stronger deformation and larger adsorption energies than for a molecule merely lying on the surface of a wide pore. Another explanation is that the photophysical properties of the positively charged dye are modified by some specific and strong interaction with the pore surface, for example, with surface hydroxyl groups.

Millimeter-sized chips of the doped monoliths were deposited in a microcavity microscope slide with a few drops of ethylene glycol for index matching, covered with a cover slip, and left to equilibrate for half an hour before observation under the microscope. From the loss of weight under vacuum drying and from the weighed uptake of ethylene glycol by the gels, we conclude that the mesopore system of both types of gel is flooded with ethylene glycol.

**2.3. Single-Molecule Detection.** Images were recorded with a wide-field imaging setup, schematically depicted in Figure 4a, in which fluorescence from individual molecules appears as diffraction-limited bright spots. Dye 9A1 was excited at 633 nm with a He–Ne laser (NEC). The laser beam is expanded, passed through a diaphragm of diameter ca. 5 mm, and focused onto the back-focal plane of a microscope objective (Nikon Plan Apo 100×/1.4 oil; the microscope stand is a Nikon eclipse TE200). The focal depth of the microscope is about 3  $\mu\text{m}$ . The fluorescence of the dye is collected by the same objective, separated from backscattered laser light with a combination of filters (dichroic mirror 640 nm cutoff, notch 633 and band-pass BP730/140 AHF), and imaged onto an intensified MCP-CCD camera (Princeton Instruments, PentaMAX-512EFT, 512  $\times$  512 px). The setup renders images with a scale of 169 nm per pixel and a frame rate of up to 28 per second (35 ms per frame,

including read-out delay of ca. 1 ms). The size of the image can be adjusted from measurement to measurement. It is usually around 30  $\mu\text{m}$   $\times$  30  $\mu\text{m}$  (180 pixels  $\times$  180 pixels). For practical reasons films are limited to 500 frames. The frame rate in the present case was 10  $\text{s}^{-1}$ , giving a total observation time of 50 s for the full film. Typical single molecules of 9A1 are visible over a time span between 1 and 10 s, depending whether the molecule vanishes due to photobleaching or diffuses out of the observation region (see below). Single molecules were not observed in undoped samples of the gels.

Sequences of images are analyzed semiautomatically with software specially developed by us to follow single-molecule fluorescence spots. Figure 4b is an example of a frame showing two molecules. The images are not subjected to any kind of data smoothing prior to analysis. The position of a molecule in frame  $n$  ( $x_n, y_n$ ) is found to higher accuracy than the diffraction limit, by fitting a two-dimensional normal fit function to the fluorescence spot, after subtracting the background signal

$$I(x,y) = A_n \exp(-((x - x_n)^2 + (y - y_n)^2)/2\sigma_n^2) \quad (1)$$

where  $A_n$  is the amplitude and  $\sigma_n$  is related to the full width (diameter) at half-maximum by  $\text{fwhm} = 2(2 \ln 2)^{1/2}\sigma_n$ . The errors in the four parameters  $A_n$ ,  $x_n$ ,  $y_n$ , and  $\sigma_n$  of eq 1 depend on the signal-to-noise ratio and on the data density<sup>39</sup> and vary for each spot. The absolute error of the coordinates  $x_n$  and  $y_n$  from all spots in the films ranges from 20 to 80 nm, with an average of 50 nm. The average error for a particular immobile molecule observed over 500 frames was 21.2 nm, in good agreement with the standard deviation of the positions, which was 22.1 nm for this molecule (cf. Figure 4d). Sufficiently dilute samples (nominal concentration  $10^{-10}$  M) were used so that the tracks of different molecules do not overlap in the same film. That would otherwise complicate correct assignment in following a molecule from frame to frame. The position of the focal plane was adjusted so that measurements were made at least at a depth of 10  $\mu\text{m}$  inside the sample.

Three reasons for molecules appearing or disappearing from the films are diffusion in and out of the focal plane, photobleaching, and possible strong interactions with the substrate, altering the photophysical properties of the molecule when it is adsorbed on the pore surface (see above). Once some molecules have been tracked, one can estimate the diffusion coefficient or coefficients (see section 3) and the distribution of track durations. We used the known geometry of the detection volume and the experimentally determined diffusion coefficients found below to evaluate the distribution of track durations in Monte Carlo simulations of the Brownian motion. In these simulations, a molecule undergoes Brownian motion in a slab centered on the focal volume, using the distribution of step lengths between frames calculated from the diffusion coefficient. Periodic boundary conditions are applied to the motion at the slab boundaries. The distribution of times spent in the detection volume can be built up from these simulations. In the case of gel M22, diffusion alone, without photobleaching, is a sufficient explanation of the distribution of track durations. Tracks last significantly longer in M3 (mean 12.3 s, standard deviation 13.6 s for trapped or immobile molecules). Because of the variety of behaviors noted below, it is not possible to tell if diffusion out of the detection volume is the only process curtailing the tracks in M3. Single molecules of 9A1 embedded in PMMA survive  $(4.4 \pm 0.7) \times 10^6$  optical cycles, to be compared with  $(4 \pm 2) \times 10^7$  for oxazine-1, or  $(4 \pm 2) \times 10^6$  for Cy5 in the same matrix.

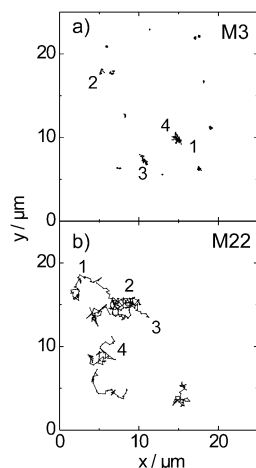


**Figure 5.** Tracks of 9A1 in M3 (a) and M22 (b). Trajectories are reconstructed from the output of the tracking software. Those appearing as superposed are in fact from the same focal region but in different films. The temporal resolution is 100 ms, and the typical time span of a track is 5 s. Numbered tracks are discussed in more detail in Figure 7.

Before discussing the results, we should recall that we are in fact sampling continuous Brownian motion at discrete times. We shall nonetheless refer to the change in position between frames as a “step” and represent the trajectories as broken lines.

### 3. Results and Discussion

**3.1. Qualitative Analysis of Single-Molecule Tracks.** Films of 500 images each were recorded for samples of M3 and M22 doped with dye 9A1 at an estimated concentration of  $10^{-10}$  M. About 10 single molecules appeared at random intervals in each of the films, usually remaining visible for 1–10 s, or 10–100 frames. In order to check the homogeneity of the monoliths, about 10 films were made in different chips of each kind of sample and at different depths within a chip. Molecular positions in each frame were determined from the fit of the two-dimensional normal function eq 1 to the fluorescence spots. Bias of the operator is always a question when evaluating single-molecule data. Therefore, we did not look for interesting regions of the sample or wait for an interesting molecule to appear to start a film. Figure 5 shows examples of single-molecule tracks from chips of samples M3 and M22, tracked in different films of the same region of the sample. Short tracks, which may result from molecules that happen to be moving in the  $z$ -direction, have been omitted for clarity in this figure.

The numbered tracks in Figure 5 will be discussed as typical examples in more detail later. A number of molecules in both types of sample were immobile at the present levels of positioning accuracy and duration of observation. It is nonetheless immediately apparent that a majority of molecules of 9A1 in M22 move several micrometers during the film, whereas a majority of those in M3 move but within a restricted area around their first sighting (note that both samples are shown at the same scale). The motion of some molecules in M3 is barely perceptible at this scale, and 20 were actually immobile to within our positioning accuracy (see below). The fraction of restricted or immobile molecules is estimated to be less than 20% in M22, whereas in M3 this proportion is significantly higher ( $\sim 80\%$ ). These first observations already indicate that diffusion of 9A1 molecules is much more efficient in the larger pores of M22 than in the smaller pores of M3.

**3.2. Global Quantitative Analysis of Tracks.** We turn now to quantitative evaluation of the data. At least three scales of

length and time can be distinguished for thermal agitation of molecules in micro- and mesoporous materials. At very short times (but long compared to molecular collision times), one expects simple Brownian motion as molecules diffuse in the liquid trapped in a pore or over the pore surface. The mean squared displacement is then proportional to time (see eq 3). At intermediate times, confinement in the pores is expected to lead to deviations from Fickian diffusion such as a time-dependent diffusion coefficient or anisotropies for individual molecules. Finally, at times such that the molecule has visited many pores, the microstructure of the material is unimportant and regular diffusion should prevail, albeit with a reduced diffusion coefficient relative to diffusion in the pure liquid filling the pores.

The positioning accuracy of the microscope used here is 15 or 2 times bigger than the size of the pores in M3 and M22, respectively, deduced from the nitrogen adsorption isotherms. The scales of length probed here are thus larger than the correlation length introduced in the Brownian motion of the molecules by the finite size of the pores. One therefore expects only weak or moderate deviations from regular diffusion in M3 and M22, respectively, such as diffusion coefficients reduced relative to diffusion in the pure solvent because of increased viscosity in the pores or because of rattling in a pore before finding the outlet. In the statistical tests of the position data from the films, our null hypothesis will therefore be regular diffusion described by Fick’s laws. In two dimensions or for the three-dimensional tracks which are projected onto a plane by the finite depth of focus of the microscope, the probability density of the presence of the particle at time  $t$  at the position vector from the first observation at time  $t = 0$  is

$$\rho(\vec{r}, t) = 1/(\pi r^2(t)) \exp(-r^2/\langle r^2(t) \rangle) \quad (2)$$

where  $r = |\vec{r}|$  and the mean squared displacement obeys

$$\langle r^2(t) \rangle = 4Dt \quad (3)$$

with the isotropic diffusion coefficient  $D$ . The distribution of displacements (“step” lengths) in time  $t$  is then

$$q(r, t) = 2r \exp(-r^2/\langle r^2(t) \rangle) / \langle r^2(t) \rangle \quad (4)$$

and that of the squared step length ( $r^2 = u$ ) is

$$p(u, t) = 1/\langle r^2(t) \rangle \exp[-u/\langle r^2(t) \rangle] \quad (5)$$

As pointed out by McCain et al.,<sup>35</sup> the diffusion coefficient can be obtained to higher accuracy from single-molecule tracks by examining the distributions of  $r$  or  $r^2$  per step rather than fitting a straight line to eq 3 with time counted from the first frame in which a molecule appears. However, close approximation of the data by eqs 4 or 5 for *one* lag  $t$  is insufficient to guarantee regular diffusion. One also has to consider the long term behavior. For example, the distribution of “step” lengths for the restricted molecules mentioned above is also well approximated by eqs 4 and 5 for lags of 1, 2, or 10 frames (see below). But for these molecules,  $\langle r^2(t) \rangle$  is stationary, instead of growing linearly with the lag  $t$ . The best way to determine  $D$  is to use the assumption implicit in modeling the movement of a molecule by Brownian motion, namely, that the process is stationary and that all intermediate positions on the track are equally valid starting points for the analysis in eqs 2–5. Equation 5 can then be used to fit  $\langle r^2(t) \rangle$  for lags  $t = \delta t, 2\delta t, \dots, m\delta t, \dots$ , and one can simultaneously check that eq 3 holds at long times and deduce the diffusion coefficient from a

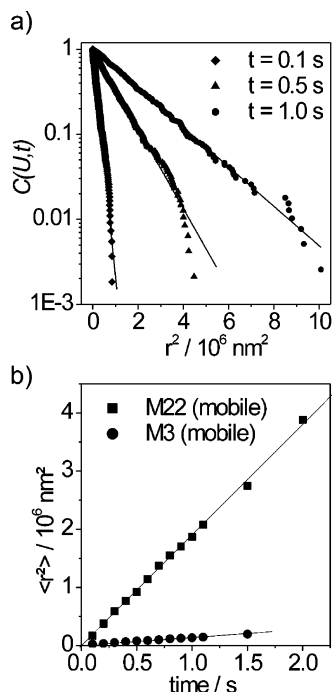


**Figure 6.** Analysis of diffusion for a fictitious average molecule in M22. (a) The mean squared displacements at given lag  $t$  in M22 are obtained by ranking all the steps with that lag from all the mobile molecules, to form the complementary cumulative probability function, eq 7. The mean squared displacements are deduced from fits to eq 7 (solid lines). (b) The linearity of the plot of mean squared displacements against time, eq 3, for M22 (squares) and M3 (circles) confirms regular diffusion, with the effective diffusion coefficients  $D_{E,M22} = 4.7 \times 10^{-9} \text{ cm}^2/\text{s}$  and  $D_{E,M3} = 3.5 \times 10^{-10} \text{ cm}^2/\text{s}$ .

fit of  $\langle r^2(t) \rangle$  versus  $t$ . Note that from a practical point of view, it is better not to lose information by binning the step data from the tracks to determine  $p(u,t)$  but to sort values of  $u = r^2$  by ascending order to form the cumulative probability distribution:<sup>40</sup>

$$P(U,t) = \int_0^U p(u,t) du = 1 - \exp(-U/\langle r^2(t) \rangle) \quad (6)$$

$P(U,t)$  is the probability that  $r^2$  does not exceed  $U$ . It can be estimated from the experimental data in the following way: if the  $j$ th out of  $N$  sorted data is  $U_j$ , then  $P(U_j,t) = j/N$ . The complementary function

$$C(U,t) = 1 - P(U,t) \quad (7)$$

is thus a simple decaying exponential (for ordinary Brownian motion). We focus below on the step lengths, but we also checked that the distribution of azimuths of individual steps for all molecules in a given gel type is indeed consistent with purely random fluctuations about the flat distribution, expected for an isotropic sample (data not shown).

Figure 6 illustrates this procedure for 9A1 in M22 gels, using data from all tracks, except immobile molecules. Molecules are counted as immobile if over the whole time for which they are visible they do not move more than the positioning accuracy, 50 nm, from their initial positions. Exclusion of immobile molecules is specially important for M3 gels, because there such tracks are numerous. This point will be discussed in more detail later. From the plots of  $C(U,t)$  versus  $U$  at times  $t = 0.1, 0.5$ , and  $1.0 \text{ s}$  one finds for M22,  $\langle r^2 \rangle = 0.170 \times 10^6 \text{ nm}^2, 0.923 \times 10^6 \text{ nm}^2$ , and  $1.87 \times 10^6 \text{ nm}^2$ . The plot of  $\langle r^2 \rangle$  versus  $t$  yields the effective or average diffusion coefficient  $D_{E,M22} = 4.7 \times$

$10^{-9} \text{ cm}^2 \text{ s}^{-1}$  for a fictitious average molecule in M22. The value for M3, is an order of magnitude smaller,  $D_{E,M3} = 3.5 \times 10^{-10} \text{ cm}^2 \text{ s}^{-1}$ . A number of factors may influence the diffusion coefficient of a molecule in a material containing both micro- and mesopores. The first is whether the molecule diffuses on average while solvated in the pore fluid ("free" diffusion) or adsorbed on the pore walls ("surface" diffusion). In the first case, factors likely to influence the apparent diffusion coefficient as measured here include the rate of diffusion in the bulk of the pore fluid and the facility of alignment of the molecular long axis with the pore axis to pass pore windows. Both these processes will slow if there is an increase of the viscosity due to a preponderance of wall–fluid interactions in narrower pores compared to wide pores. Surface diffusion is also expected to be slower in the narrow pore gel because of the increase of surface area to be explored in order to make a "step" of given length in either gel. It is not possible at the moment to distinguish the contributions of these processes in our data.

**3.3. Quantitative Analysis of Individual Single-Molecule Tracks.** The data obtained so far were derived for the entire ensemble of observed molecules, distinguishing only diffusing and confined populations. We next turn to an analysis of individual tracks, revealing different behavior for different molecules in the same sample and even different behaviors for a given molecule at different times. Figure 7 shows four representative tracks for both types of sample (note the very different scales). The tracks in M22 look very much like Brownian motion tracks. Apart from the already mentioned difference in the diffusivity, the tracks in M3 also appear to be more heterogeneous. Six out of 62 molecules in M3 showed alternating periods of what appeared to be regular diffusion, interrupted by periods during which the molecule appeared to be trapped in a region a few hundred nm in diameter (see Figure 7b). Nineteen molecules were confined to similar-sized regions, without the diffusive periods. They disappeared through photobleaching or diffusion out of the focal plane. Twenty were immobile to within our positioning accuracy and six displayed what appeared to be ordinary diffusion without trapping. The remaining 11 molecules were observed too briefly to determine their type. Similar but less pronounced trapping regions are also visible in the tracks in M22, Figure 7a. It is therefore necessary to check whether the trappings are statistically significant or just an impression caused by natural fluctuations.

Starting with M22, we have picked out, as an example, track number 1 in Figure 5 and Figure 7. This track is shown again in Figure 8a. The molecule starts at the upper right side and was followed for 57 steps or 5.7 s so that good statistics are attained. Two types of analysis have been used to characterize the diffusion of *each* molecule. The simplest thing one can do is to evaluate the mean squared displacement for each lag  $t$ . This standard approach is not sensitive to different components of the mobility. The plot of these mean squared displacements against time is shown in Figure 8b. A better approach is to perform the same analysis per molecule as was done in section 3.2 for all diffusing molecules in Figure 6. Figure 8c thus shows the complementary distribution of the squared displacement,  $C(U,t)$ , i.e., the probability that the squared step exceeds  $U$  for lag  $t$ . The plot is shown for three lags, 0.2, 0.4, and 0.9 s. The linearity of the semilog plots indicates that only one component is present in the exponential decay of the probability distribution. This is consistent with a single distribution of step lengths derived from a single value of  $D$  for the whole of the track of the molecule. Values of the mean squared displacement for this molecule were obtained for all possible lags  $t$  and plotted in



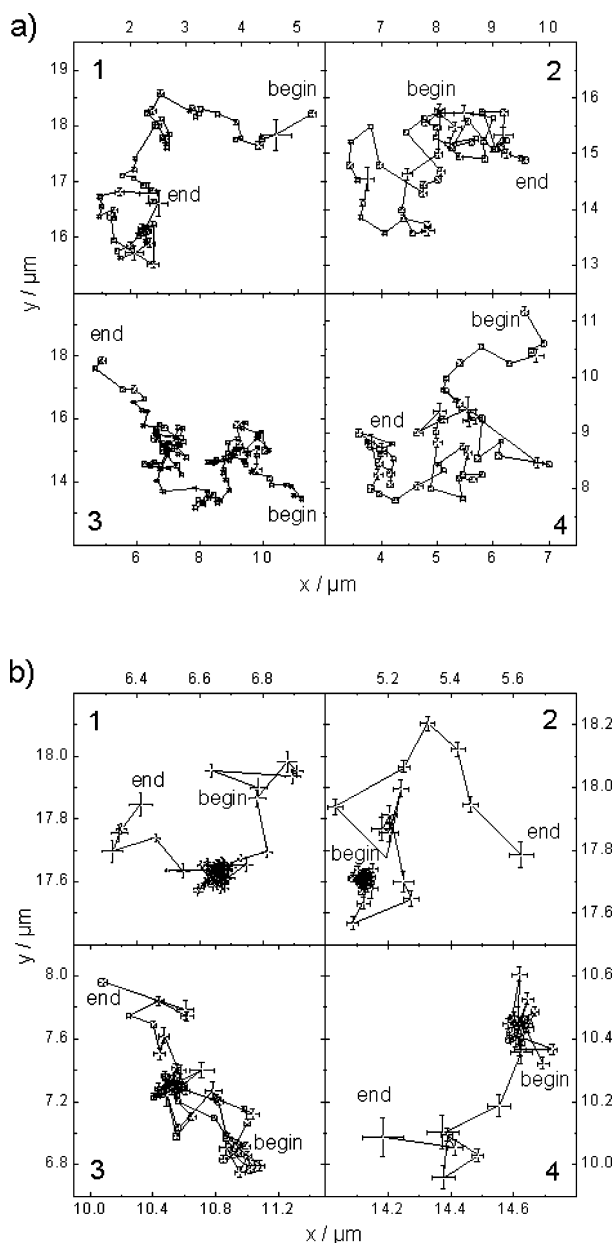


**Figure 7.** Four representative tracks of diffusing molecules in both samples M22 (a) and M3 (b). The tracks in M22 look very much like Brownian motion. The tracks in M3 show alternate free diffusion and trapping (dense clouds of data points), which last for several seconds.

Figure 8b. Linearity is clear and gives  $D_E = 3.7 \pm 0.5 \times 10^{-9} \text{ cm}^2 \text{ s}^{-1}$  for this track. The behavior of the molecule is thus consistent with Fickian diffusion. The good agreement of this plot with the plot of the mean squared displacements is a further indication that only one component of mobility is present in this trajectory.

It is in principle equivalent to look for heterogeneities within one track by analyzing the distribution of step lengths  $r$ , rather than their squares. A histogram of the step lengths of this molecule for lag  $t = 0.1 \text{ s}$  is provided for comparison in Figure 8d. Fickian diffusion would lead to the distribution  $q(r, t)$ , eq 4, and the cumulative probability function  $Q(r, t) = P(r^2, t)$  could be used again to avoid binning the data. However, the linearity of the semilog plots in part c of the figure is in our view a simpler and sensitive test of conformity with Fickian diffusion.

An analogous analysis was carried out for molecules diffusing in M3. In this case we have taken track 1 in Figure 9a as an example, since it exhibits obvious changes in diffusivity along

the way. The molecule starts at the upper right corner, diffuses for about 1 s, and is then found localized in a small region of diameter of about 100 nm for nearly 6 s, after which it is released from this confinement and diffuses for another 0.5 s before it is lost. Using the simple average to obtain the mean square displacement, and thus losing the sensitivity to the presence of different components of mobility, one obtains a diffusion coefficient of  $D_E = 9.6 \pm 1.1 \times 10^{-11} \text{ cm}^2 \text{ s}^{-1}$  (cf. Figure 9b). In fact, all steps over 100 nm (or twice the positioning accuracy) were made outside the trapping region, suggesting two types of motion. Analysis according to  $C(U, t)$ , eq 7, is useful to decide the significance of such data. The probability distribution of the squared displacements (in Figure 9c) clearly shows two decay components indicating two types of mobility. The curve is well fitted by a biexponential decay giving two values for the mean square displacements for each lag, one for the low- and one for the high-mobility components. The plot of the mean squared displacement as a function of time is shown in Figure 9b, resulting in two straight lines. The first gives  $D_M = 3.3 \pm 0.3 \times 10^{-10} \text{ cm}^2 \text{ s}^{-1}$ . The other component of the mean squared displacement is a constant value of  $2400 \text{ nm}^2$ . This value is comparable to what results from our positioning accuracy of 50 nm ( $2500 \text{ nm}^2$ ). Therefore we conclude that the regular diffusion of this molecule is indeed interrupted by a trap with a diameter  $\leq 50 \text{ nm}$ : the analysis proves that the cluster of points in the track is not just a statistical fluctuation in the Brownian motion. Since our spatial resolution is limited we cannot distinguish between an adsorption trap where the molecule may be localized on a molecular scale, for example, by momentary bonding to the silica surface, and confinement in a small trap, such as a narrow pore like a blind alley with a diameter below 50 nm, in which the molecule is still mobile. The much lower frequency of such small traps in M22 is a strong indication that those observed in M3 are indeed a spatial confinement, rather than an adsorption site, because it is thought that the surface state of amorphous silica, particularly the average surface density of silanols that might bind to the dye, is on average rather insensitive to the method of preparation.<sup>41</sup>

The distribution of the step size of this molecule is shown Figure 9d. The bimodal distribution of steps is not evident from this histogram but does appear in the cumulative distribution (upper panel of Figure 9d), where two Gaussian components are needed to fit the data. A final point is the spur to the lower left of the trapping region, which was visited twice during the trapping episode. We tentatively ascribe it to a dead end in the pore system. Similar features have been seen in other tracks (data not shown).

### 3.4. Significance of Fluctuations of $D$ for Short Tracks.

Unfortunately, it often happens that, either through photobleaching or fast diffusion, single-molecule tracks are too short to deduce reliable diffusion coefficients from fitting a straight line to  $\langle r^2(t) \rangle$  versus  $t$ . One must then use just the distribution of jumps for one step. In order to test the reliability of this method, we calculated values of the diffusion coefficient  $D$  for a sample of 42 molecules in M22 (two films), by fitting  $C(U, t)$  to the experimental distributions at lag 0.1 s. The mean of the 42 single-molecule diffusion coefficients is  $5.6 \times 10^{-9} \text{ cm}^2 \text{ s}^{-1}$ , with a standard deviation of  $2.7 \times 10^{-9} \text{ cm}^2 \text{ s}^{-1}$ . Figure 10 shows the distribution of  $D$ . The histogram is skewed, with a tail of apparently fast diffusing molecules and a spread of values comparable to the mean value. But before concluding that the material is heterogeneous, one should consider the significance of the differences in  $D$ . Thus, the accuracy of the measurement of  $D$  cannot be better than the spread of values caused by

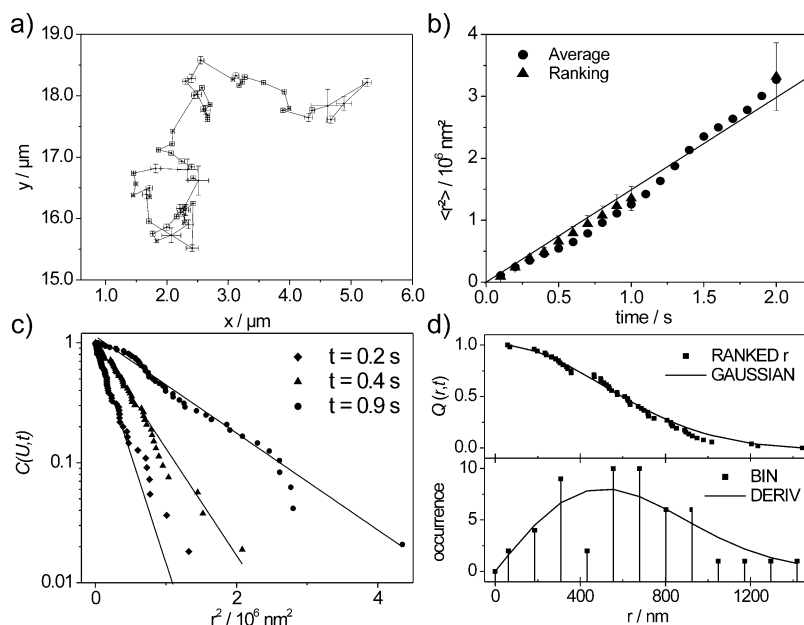


**Figure 8.** Analysis of a single-molecule trajectory in M22. (a) Individual tracks in M22 do not show pronounced inhomogeneities. In this example (track starts upper right), the molecule was followed for 5.7 s. (b) The diffusion coefficient, calculated from the time dependence of the mean squared displacements for this track (circles), is  $D_E = 3.7 \times 10^{-9} \text{ cm}^2 \text{ s}^{-1}$ . The error bars are given by  $r^2 N^{-1/2}$  with  $N$  being the total number of steps at each time lag (cf. ref 23). (c) Monoexponential decay in the population analysis of the ranked squared displacements, eq 7, confirms that a single diffusion constant holds over the whole track and yields the same value of  $D$  as in (b). (d) The step size distribution, eq 4 and lower panel here, is also described by a single value of  $D$ . The complementary cumulative distribution (upper panel) is well fitted by a single normal curve.

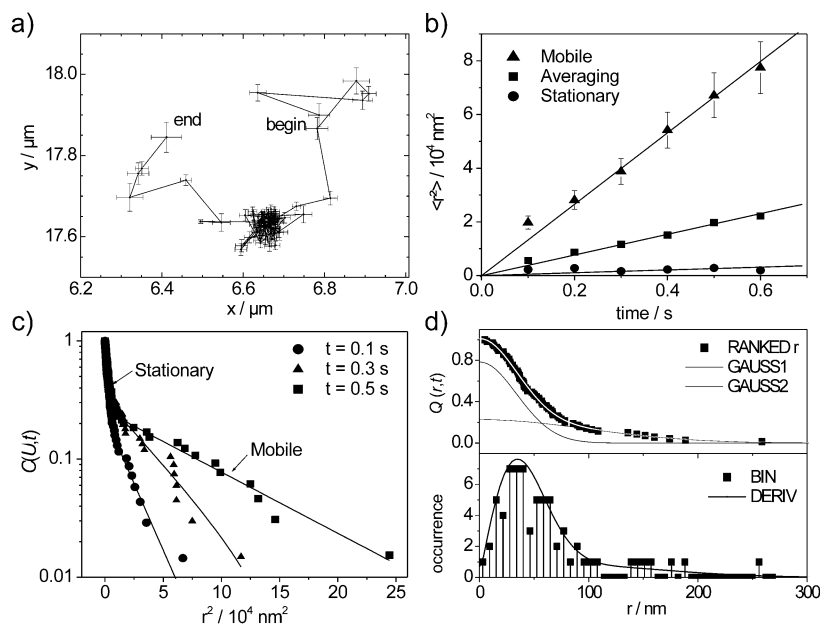


**Figure 9.** Analysis of a trajectory of a single molecule in M3. (a) Individual trajectories of 9A1 in M3 show pronounced heterogeneities. In this track (starts top right) a molecule diffuses about 1 s, gets trapped for 6 s and then escapes; the total number of steps is 69. (b) On calculating the mean squared displacements from all steps in the track and plotting against lag (squares), one finds an average diffusion coefficient  $D_E = 9.6 \times 10^{-11} \text{ cm}^2 \text{ s}^{-1}$ . (c) Population analysis of the mean squared displacements reveals two populations of steps, corresponding to the periods of free diffusion and trapping. Part b also shows the two mean squared displacements from a biexponential fit to the complementary cumulative probability, with two values of the diffusion coefficient,  $D_M = 3.3 \times 10^{-10} \text{ cm}^2 \text{ s}^{-1}$  for free diffusion of this molecule (triangles) and  $D_N \sim 1 \times 10^{-11} \text{ cm}^2 \text{ s}^{-1}$  for the trapping event. The constant value of the mean squared displacement for the second component is below the value from positioning errors, 2500 nm<sup>2</sup>, indicating that the molecule is stationary to within the experimental accuracy. (d) The bimodal distribution of steps is not quite evident from the histogram (lower panel) but does appear in the cumulative distribution (upper panel), where two Gaussian components are needed to fit the data.

statistical fluctuations when fitting the cumulative probability function to data sets for diffusion with a known constant value of  $D$ . We used Monte Carlo simulations of Fickian diffusion to prepare 500 synthetic data sets of 7 steps (the shortest of the 42 experimental tracks is considered, being the worst case) with a constant value of the diffusion coefficient, the mean value found above,  $5.6 \times 10^{-9} \text{ cm}^2 \text{ s}^{-1}$ . We then fitted  $D$  via the

cumulative probabilities for  $r$  (or  $r^2$ , the result is the same) for lag 0.1 s. Figure 10b shows the histogram of the fitted values. The same was done for a mixture of 500 track lengths in the same proportions as the experimental data. Even in the latter case, the half-width at half-maximum of the distribution is about  $1.5 \times 10^{-9} \text{ cm}^2 \text{ s}^{-1}$ , or 30% error. The error can be as high as 100% for short tracks. Nonetheless, when the experimental



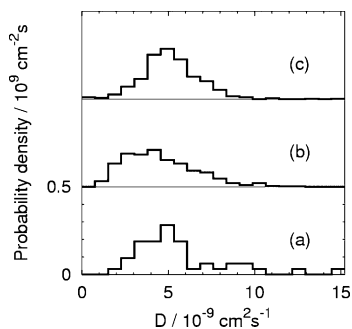


**Figure 10.** Histograms of experimentally measured and synthetically produced diffusion coefficients. (a) Distribution of the diffusion coefficients  $D$  for 42 molecules of 9A1 in gel M22. Data from a fit of eq 6 and application of eq 3 for a single lag (0.1 s). The mean for this set of molecules is  $D_m = 5.6 \times 10^{-9} \text{ cm}^2 \text{ s}^{-1}$ . (b) Distribution calculated from mere statistical fluctuations in synthetic data with a single value of  $D = D_m$ , for 500 molecules with a track length of seven steps (worst case in experimental data). (c) From synthetic data with the experimental spread of track lengths.

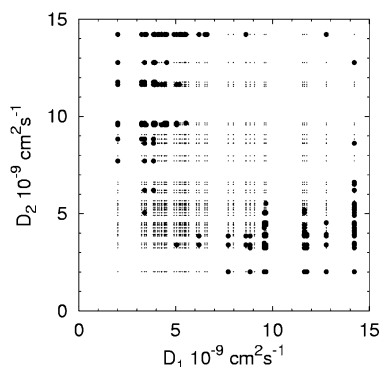


**Figure 11.** Scatter diagram of all significantly different distributions of step lengths (Kolmogorov–Smirnov test, 1% level) for pairs in a sample of 42 molecules in M22, represented by their diffusion coefficients  $D_1$  and  $D_2$ . Small crosses, all pairs of  $D$ ; spots, pairs of  $D$  for molecules with significantly different step lengths.

histogram was compared with the synthetic one with the same distribution of track lengths, it was found that the distributions differ at the 5% level of the Kolmogorov–Smirnov test,<sup>42</sup> adding to our confidence that the tail of fast molecules is a real effect.

Finally, we cross-checked the cumulative distributions of step lengths of all *pairs* of molecules. The Kolmogorov–Smirnov test showed numerous significant differences at the 1% level, for pairs of molecules with diffusion coefficients on opposite sides of the distribution of  $D$  (see Figure 11). This confirms the initial impression of heterogeneity and a 5-fold range of the diffusion coefficient. Note that although molecules are represented by their  $D$  values in Figure 10, the test bears on the raw step data. This is perhaps more satisfactory than comparing  $D$ 's from a fit of  $\langle r^2(t) \rangle$  versus  $t$  for short trajectories, where values and errors are to some extent dependent on the fitting criterion, such as the maximum or mean absolute deviation or the total squared deviation. We note in passing that the mean value of  $D$  in Figure 10,  $5.6 \times 10^{-9} \text{ cm}^2 \text{ s}^{-1}$ , differs from the value of  $4.7 \times 10^{-9} \text{ cm}^2 \text{ s}^{-1}$  found above from all steps of all diffusing molecules, both because the data are a subset of those used above and because they are not used the same way.

Using this analysis, one can estimate the diffusion coefficient of the free fraction of molecules in M3 by excluding the trapping episodes from the cumulative probability distributions of  $r^2$  of individual molecules, as above. We find a mean value of  $1.2 \times 10^{-9} \text{ cm}^2 \text{ s}^{-1}$ , or about 5 times smaller than in M22 ( $5.6 \times$

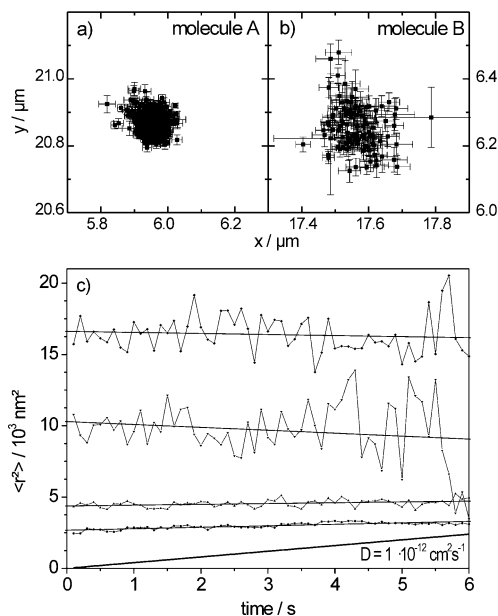


**Figure 12.** Examples of nondiffusing molecules in M3 (both plots 600 nm full scale). (a) The jittering of molecule A is less than the positioning accuracy (50 nm), whereas that of molecule B is significantly larger (b). The mean squared displacements for these molecules and two others are shown in (c). All four diffusion coefficients are below detection (straight line at the bottom). The two tracks with the largest vertical offsets correspond to confinement in traps with cross sections of  $10\,000 \text{ nm}^2$  and  $16\,500 \text{ nm}^2$ .

$10^{-9} \text{ cm}^2 \text{ s}^{-1}$ ), albeit with a much smaller sample. Although the sample is small, we note that as in M22 there is a wide spread of the values of  $D$ , the standard deviation being  $7.1 \times 10^{-10} \text{ cm}^2 \text{ s}^{-1}$  and there are significant differences (1% level of the Kolmogorov–Smirnov test) between the smallest and largest values ( $3.8 \times 10^{-10} \text{ cm}^2 \text{ s}^{-1}$  and  $2.3 \times 10^{-9} \text{ cm}^2 \text{ s}^{-1}$ ).

**3.5. Confined Molecules.** We recall that a large majority of the molecules in M3 were trapped or immobile over the whole time they were visible. Two different cases of 9A1 in M3 are shown in Figure 12a and b. The corresponding mean squared displacements are plotted as a function of time in Figure 12c, together with two additional molecules in M3. The mean squared displacements of these molecules are effectively constant and have offsets of the ordinate of  $2400 \text{ nm}^2$  for molecule A and  $10^4 \text{ nm}^2$  for trajectory B. As already discussed, our positioning accuracy is about 50 nm giving a resolvable  $r^2$  above  $2500 \text{ nm}^2$ . Thus molecule A is immobile to within our resolution, whereas the other three molecules are diffusing in cages with cross sections in the focal plane between  $4500 \text{ nm}^2$  and  $16\,500 \text{ nm}^2$ . An expression for a random walk in a confinement<sup>24</sup> gives a time dependence of the MSD according to

$$\langle r^2(t) \rangle = r_c^2 [1 - \exp(-BDt/r_c^2)] \quad (8)$$

with an asymptote  $\langle r^2(t) \rangle = r_c^2$ . This asymptotic behavior is characterized by the effective diameter  $r_c$  of the confinement. Due to the limited temporal resolution, we cannot see the ascending component in our plot corresponding to eq 8 in which the factor  $B$  accounts for the corral geometry. We therefore do not obtain a diffusion coefficient; however, we can obtain the asymptotic value  $r_c^2$  for the size of the confinement.

The smallest resolvable diffusion coefficient depends on the observation time and the positioning accuracy. Under the assumption that a molecule can be observed for a period of at least 6 s and with a positioning accuracy of 50 nm, the resulting diffusion coefficient is about  $10^{-12} \text{ cm}^2 \text{ s}^{-1}$ . In the case of

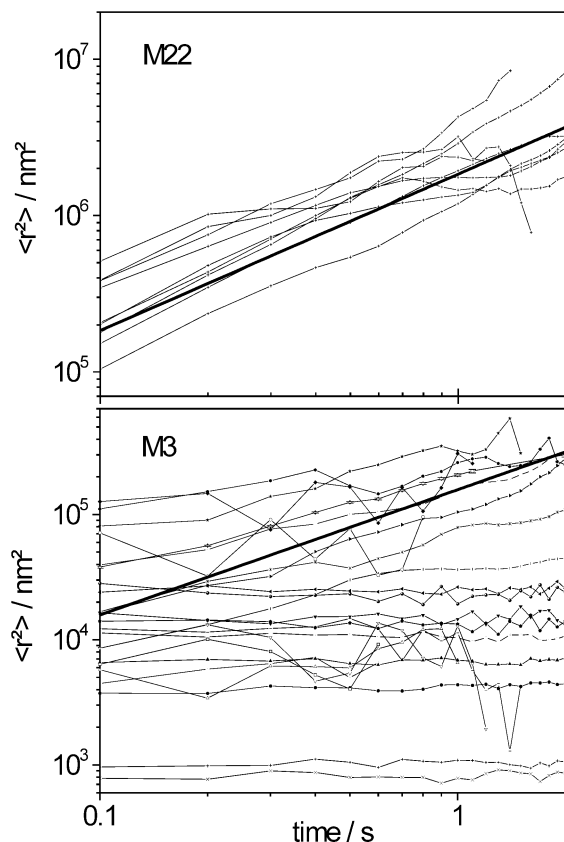


**Figure 13.** Sample mean squared displacements for 9A1 in gels M3 and M22. Mean squared displacement plots of individual molecules, in M3 (bottom) and M22 (top), compared to that of the fictitious average molecules in Figure 6 (straight lines). A wide ( $5\times$ ) spread of the diffusion coefficients for individual molecules is present in both samples. In M3 there are also a majority of trapped molecules with constant mean squared displacements.

localized molecules (Figure 12) we see that the detected diffusion coefficient lies below this number (see the straight line at the bottom of the plot).

Figure 13 shows the mean squared displacements of a sample of the mobile molecules in M3 and M22. Considering first M22, the linearity of the log–log plots with slope unity confirms that all move consistently with a regular diffusion process. On the other hand the vertical offsets of the different graphs show the spread of diffusion coefficients from one molecule to another confirming the spread of  $D$  deduced from analysis of the step distributions in section 3.4. The plots for individual molecules in M22 are spread around the mean value determined above by combining data from all molecules (straight line in Figure 13). The plots for M3 are of two kinds, those from diffusing molecules, with nonzero slope, and those for the localized molecules, which are parallel to the time axis. With better temporal and spatial resolution one should in principle hope to see a rise of  $\langle r^2(t) \rangle$  for the latter at short times.

It is difficult to compare our data with earlier work. The silica thin films in which McCain et al.<sup>35</sup> observed single rhodamine 6G molecules were not dried like ours, and no pore diameter could be reported. The diffusion coefficients found there were of the same order of magnitude as in M3, and as in M3, diffusion of the majority of molecules could not be seen because of trapping. Their method of synthesis was by base catalysis with a large excess of water (about 1/10 tetraethyl orthosilicate/water). On the other hand, Wang et al.<sup>43</sup> also prepared silica films with a large excess of water but in acid conditions. Using confocal microscopy, these authors also reported that the majority of

molecules were trapped in their samples. Mei et al.<sup>32</sup> did not mention motion of rhodamine 6B in thin silica films prepared with a similar composition. In view of the sensitivity of silica gels to the precise methods of synthesis, we therefore think that it would be useful in future work to examine several dyes in a homogeneous series of monoliths with known, graduated porosities.

#### 4. Conclusion

A newly synthesized streptocyanine dye is found to be sufficiently photostable for single-molecule measurements in silica xerogels. It is one of a family of dyes with graduated spectral properties, shapes and sizes, which may prove useful to study the influence of these parameters on molecular diffusion in a variety of systems, including biological samples, since long trajectories have been observed. Tracking of single molecules was applied here to two cast monolith silicas, M3 and M22, both with micro- and mesopores, differing mainly in their mesoporosity. The mean mesopore diameters were about 3 and 22 nm, respectively, according to nitrogen adsorption/desorption isotherms. Sol–gel materials for single-molecule or fluorescence correlation measurements have previously been prepared as thin films, which helps to reduce the sample volume and to limit scattering detrimental to the signal-to-noise ratio of single-molecule detection. The synthesis method developed here leads to transparent, crack-free monoliths in which single molecules are readily visible in the bulk of the sample, whereas in the case of thin films, attention must be paid to exclude the possibility that some molecules may be diffusing at the liquid–solid interface.

In the sol–gel with narrower pores, the dye was found largely (80%) trapped in regions of diameter from below the positioning accuracy of the microscope, 50 nm, to about 200 nm. Much evidence shows that the surface of amorphous silica, particularly the surface density of silanols that might bind to the dye, is on average insensitive the method of preparation.<sup>41</sup> Since the traps are much rarer in M22 than in M3, we conclude that they probably are physical traps rather than chemical bonding to the surface. Observation of a dead end next to one of the traps in M3 is in agreement with this point. Detection of such nondiffusing molecules is one of the advantages of single-molecule detection compared to fluorescence correlation spectroscopy. Other molecules diffused with a diffusion coefficient of about  $1.2 \times 10^{-9} \text{ cm}^2 \text{ s}^{-1}$ . Some showed alternately diffusion and trapping.

In the silica with wider pores, motion of most molecules was consistent with Fickian diffusion, over ranges of the order of 5  $\mu\text{m}$  in a few seconds or so, with a diffusion coefficient of the order of  $4.7 \times 10^{-9} \text{ cm}^2 \text{ s}^{-1}$ . Some molecules (20%) also showed trapping. Both silicas show about a 5-fold spread of the diffusion coefficient for different molecules. Monte Carlo simulations were employed to prove the significance of the results and to find that for this gel most tracks were probably terminated by the molecule moving out of the detection volume, not by photobleaching.

Single-molecule tracking is thus a powerful tool to pinpoint nanoscale heterogeneities in complex systems such as sol–gel materials. It is to be hoped that further studies will address these systems and other molecular sieves such as nanoporous zeolites.

**Acknowledgment.** The authors thank the SFB486 of the Deutsche Forschungsgesellschaft for financial support.

#### References and Notes

- (1) Pandey, P. C.; Upadhyay, S.; Pathak, H. C. *Sens. Actuators, B* **1999**, 60, 83.

- (2) Weiss, Ö.; Loerke, J.; Wüstefeld, U.; Marlow, F.; Schüth, F. *J. Solid State Chem.* **2002**, *167*, 302.
- (3) Reisfeld, R. *J. Lumin.* **1997**, *72*, 7.
- (4) Yang, P.; Wirnsberger, G.; Huang, H. C.; Cordero, S. R.; McGehee, M. D.; Scott, B.; Deng, T.; Whitesides, G. M.; Chmelka, B. F.; Buratto, S. K.; Stucky, G. D. *Science* **2000**, *287*, 465.
- (5) Darracq, B.; Chaput, F.; Lahli, K.; Boilot, J. P.; Levy, Y.; Alain, V.; Ventelon, L.; Blanchard-Desce, M. *Opt. Mater.* **1998**, *9*, 265.
- (6) Soggiu, N.; Cardy, H.; Habib Jiwan, J. L.; Leray, I.; Soumillion, J. P.; Lacombe, S. *J. Photochem. Photobiol., A* **1999**, *124*, 1.
- (7) Jenny, C.; Maddox, P. *Curr. Opin. Solid State Mater. Sci.* **1998**, *3*, 94.
- (8) Kukla, V.; Kornatowski, J.; Demuth, D.; Girnus, I.; Pfeifer, H.; Rees, L. V. C.; Schunk, S.; Unger, K. K.; Kärger, J. *Science* **1996**, *272*, 702.
- (9) Jobic, H.; Bee, M.; Karger, J.; Vartapetian, R. S.; Balzer, C.; Julbe, A. *J. Membr. Sci.* **1995**, *108*, 71.
- (10) Benes, N. E.; Jobic, H.; Verweij, H. *Microporous Mesoporous Mater.* **2001**, *43*, 147.
- (11) Björnström, J.; Martinelli, A.; Johnson, J. R. T.; Matic, A.; Panas, I. *Chem. Phys. Lett.* **2003**, *380*, 165.
- (12) Bartolotta, A.; Carini, G.; D'Angelo, G.; Fontana, A.; Rossi, F.; Tripodo, G. *J. Non-Cryst. Solids* **1999**, *245*, 9.
- (13) Geddes, C. D.; Birch, D. J. S. *J. Non-Cryst. Solids* **2000**, *270*, 191.
- (14) Hungerford, G.; Pereira, M. R.; Ferreira, J. A.; Viseu, T. M. R.; Coelho, A. F.; Isabel, M.; Ferreira, C.; Suhling, K. *J. Fluoresc.* **2002**, *12*, 397.
- (15) Tozuka, Y.; Tashiro, E.; Yonemochi, E.; Oguchi, T.; Yamamoto, K. *J. Colloid Interface Sci.* **2002**, *248*, 239.
- (16) Klonek, A. M.; Kledzik, K.; Ostaszewski, R.; Widernik, T. *Colloids Surf., A* **2002**, *208*, 115.
- (17) Weiss, A. M.; Saraidarov, T.; Reisfeld, R. *Opt. Mater.* **2001**, *16*, 15.
- (18) Brinker, C. J.; Scherer, G. W. *Sol–Gel Science: The Physics and Chemistry of Sol–Gel Processing*; Academic Press: San Diego, 1990.
- (19) Elson, E. L.; Madge, D. *Biopolymers* **1974**, *13*, 1.
- (20) Rigler, R.; Mets, U.; Widengren, J.; Kask, P. *Eur. Biophys. J.* **1993**, *22*, 169.
- (21) Schwill, P.; Haupts, U.; Maiti, S.; Webb, W. W. *Biophys. J.* **1999**, *77*, 2251.
- (22) Schmidt, T.; Schutz, G. J.; Baumgartner, W.; Gruber, H. J.; Schindler, H. *Proc. Natl. Acad. Sci. U.S.A.* **1996**, *93*, 2926.
- (23) Qian, H.; Scheetz, M. *Biophys. J.* **1991**, *60*, 910.
- (24) Saxton, M. J.; Jacobson, K. *Annu. Rev. Biophys. Biomol. Struct.* **1997**, *29*, 373.
- (25) Seisenberger, G.; Ried, M. U.; Endress, T.; Büning, H.; Hallek, M.; Bräuchle, C. *Science* **2001**, *294*, 1929.
- (26) Orrit, M.; Bernard, J.; Brown, R.; Lounis, B. *Prog. Opt.* **1996**, *35*, 61.
- (27) Nie, S.; Zare, R. N. *Annu. Rev. Biophys. Biomol. Struct.* **1997**, *26*, 567.
- (28) Tamarat, P.; Maali, A.; Lounis, B.; Orrit, M. *J. Phys. Chem. A* **2000**, *104*, 1.
- (29) Seebacher, C.; Hellriegel, C.; Bräuchle, C.; Ganschow, M.; Wöhrle, D. *J. Phys. Chem. B* **2003**, *107*, 5411.
- (30) Wirth, M. J.; Swinton, D. J.; Ludes, M. D. *J. Phys. Chem. B* **2003**, *107*, 6258.
- (31) Wirth, M. J.; Swinton, D. J. *Anal. Chem.* **1998**, *70*, 5264.
- (32) Mei, E.; Bardo, A. M.; Collinson, M. M.; Higgins, D. A. *J. Phys. Chem. B* **2000**, *107*, 9973.
- (33) Mahurin, S. M.; Dai, S.; Barnes, M. D. *J. Phys. Chem. B* **2003**, *107*, 13336.
- (34) Seebacher, C.; Hellriegel, C.; Deeg, F. W.; Bräuchle, C.; Müllen, K.; Altmaier, S.; Behrens, P. *J. Phys. Chem. B* **2002**, *106*, 5591.
- (35) McCain, K. S.; Hanley, D. C.; Harris, J. M. *Anal. Chem.* **2003**, *75*, 4351.
- (36) Madaule, Y.; Payrastra, C.; Izquierdo, A. *Chem. Abstr.* **2002**, *137*, 17444.
- (37) Izquierdo, A.; Guieu, V.; Gornitzka, H.; Madaule, Y.; Payrastra, C. *Eur. J. Org. Chem.*, in press.
- (38) Brunauer, S.; Deming, L. S.; Deming, W. S.; Teller, E. *J. Am. Ceram. Soc.* **1940**, *62*, 1723.
- (39) Bobroff, N. *Rev. Sci. Instrum.* **1986**, *57*, 1152.
- (40) Sonnleitner, A.; Schutz, G. J.; Schmidt, T. *Biophys. J.* **1999**, *77*, 2638.
- (41) Zhuravlev, L. T. *Colloids Surf., A* **2000**, *173*, 1.
- (42) Press, W. H.; Flannery, B. P.; Teukolsky, S. A.; Vetterling, W. T. *Numerical Recipes*; Cambridge University Press: Cambridge, 1986.
- (43) Wang, H.; Bardo, A. M.; Collinson, M. M.; Higgins, D. A. *J. Phys. Chem. B* **1998**, *102*.
- (44) Brunauer, S.; Emmet, P. H.; Teller, E. *J. Am. Chem. Soc.* **1938**, *60*, 309.
- (45) Horvath, G.; Kawazoe, K. *J. Chem. Eng. Jpn.* **1983**, *16*, 470.
- (46) Barrett, E. P.; Joyner, L. G.; Halenda, P. H. *J. Am. Chem. Soc.* **1951**, *73*, 373.